The Continuous Spectrum of Periodically Stationary Pulses in a Stretched Pulse Laser

In this document we provides supplementary material for "The Continuous Spectrum of Periodically Stationary Pulses in a Stretched Pulse Laser". We first demonstrate how the periodically stationary pulse breathes over one round trip in the laser. Then, we provide a derivation of linearization of the round trip operator, $\mathcal{R}$, about a pulse, ψ. Finally, we present some additional numerical results to support the theory developed in the paper.

1. BREATHING OF A PULSE OVER ONE ROUND TRIP

In Fig. S1, we show how the periodically stationary pulse breathes over one-round trip of the laser. These results were obtained using the parameter set with the stronger saturable absorber ($\ell_0 = 0.2$, $P_{\text{sat}} = 50$ W). We plot the amplitude of the pulse exiting each component of the laser. We observe that the pulse undergoes significant changes before returning to its original shape at the end of the round trip.

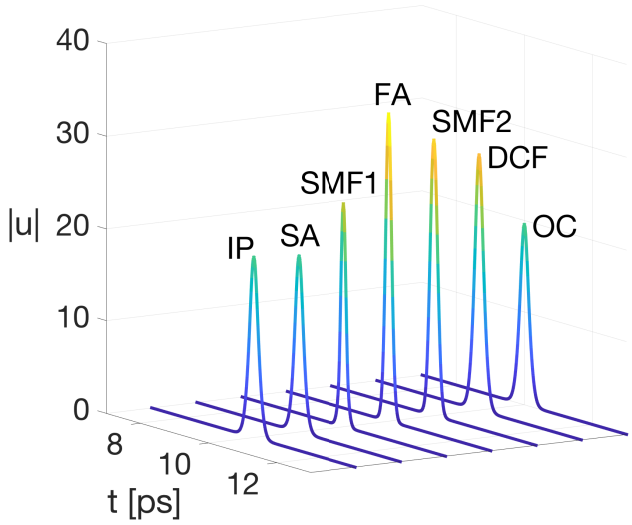

Fig. S1. Plot of the periodically stationary pulse associated with parameter set 2 showing the amplitude of the pulse exiting each component of the laser.

2. LINEARIZATION OF THE ROUND TRIP OPERATOR

As in Eq. (1) of the paper, we define the round trip operator, $\mathcal{R}$, to be the composition of the transfer functions of all the components of the laser given by

$$\mathcal{R} = \mathcal{P}^{\text{OC}} \circ \mathcal{P}^{\text{DCF}} \circ \mathcal{P}^{\text{SMF2}} \circ \mathcal{P}^{\text{FA}} \circ \mathcal{P}^{\text{SMF1}} \circ \mathcal{P}^{\text{SA}}. \tag{S1}$$

Here, we regard each transfer function, $\mathcal{P}$, as acting on a column vector of the form $\boldsymbol{\psi} = [\text{Re}\,\psi, \text{Im}\,\psi]^T = [\psi_1, \psi_2]^T$, where ψ is a complex valued function of t. By the chain rule, the linearization of $\mathcal{R}$ about a pulse, $\boldsymbol{\psi}$, is a composition of the linearizations, $\mathcal{U}$, of the individual transfer functions, $\mathcal{P}$. Therefore, the monodromy operator, $\mathcal{M}$, is given by

$$\mathcal{M} = \mathcal{U}^{\text{OC}} \circ \mathcal{U}^{\text{DCF}} \circ \mathcal{U}^{\text{SMF2}} \circ \mathcal{U}^{\text{FA}} \circ \mathcal{U}^{\text{SMF1}} \circ \mathcal{U}^{\text{SA}}. \tag{S2}$$

Because eigenvalues and eigenvectors can be complex, we regard the transfer functions, $\mathcal{U}$, as acting on the column vectors of the form $\boldsymbol{u} = [u_1, u_2]^T$, where each u_j is a complex valued function of t.

We first derive the linearized transfer function, $\mathcal{U}^{\text{FA}}$, corresponding to the transfer function, $\mathcal{P}^{\text{FA}}$, of the fiber amplifier about ψ. We rewrite the transfer function, $\mathcal{P}^{\text{FA}}$, of a fiber amplifier of length, L_{FA}, in terms of $\boldsymbol{\psi} = (\psi_1, \psi_2)$ as

$$\boldsymbol{\psi}_{\text{out}} = \mathcal{P}^{\text{FA}} \boldsymbol{\psi}_{\text{in}}, \tag{S3}$$

where $\boldsymbol{\psi}_{\text{out}}(t) = \boldsymbol{\psi}(\text{L}_{\text{FA}}, t)$ is obtained by solving the initial value problem

$$\begin{aligned} \partial_z \boldsymbol{\psi} &= \left[\tfrac{g(\boldsymbol{\psi})}{2} \left(1 + \tfrac{1}{\Omega_g^2} \partial_t^2 \right) - \tfrac{\beta}{2} \mathbf{J} \partial_t^2 + \gamma(\psi_1^2 + \psi_2^2)\mathbf{J} \right] \boldsymbol{\psi}, \\ \boldsymbol{\psi}(0, t) &= \boldsymbol{\psi}_{\text{in}}(t). \end{aligned} \tag{S4}$$

Here, $\mathbf{J} = \begin{bmatrix} 0 & -1 \\ 1 & 0 \end{bmatrix}$ and $g(\boldsymbol{\psi})$ is the saturable gain given by

$$g(\boldsymbol{\psi}) = \tfrac{g_0}{1 + \int_{-\infty}^{\infty} (\psi_1^2(t) + \psi_2^2(t)) dt / E_{\text{sat}}}. \tag{S5}$$

We use a perturbation, $\boldsymbol{\psi}_\epsilon = \boldsymbol{\psi} + \epsilon \boldsymbol{u}$, about $\boldsymbol{\psi}$ to linearize $\mathcal{P}^{\text{FA}}$. Throughout the following calculation, we ignore the terms of order ϵ^2 and higher. Using Eq. (S4) for both $\boldsymbol{\psi}$ and $\boldsymbol{\psi}_\epsilon$, we obtain

$$\begin{aligned} \partial_z \boldsymbol{u} &= \lim_{\epsilon \to 0} \tfrac{\partial_z \boldsymbol{\psi}_\epsilon - \partial_z \boldsymbol{\psi}}{\epsilon} \\ &= \lim_{\epsilon \to 0} \tfrac{1}{\epsilon} \left\{ \tfrac{g(\boldsymbol{\psi}_\epsilon)}{2} \left(1 + \tfrac{1}{\Omega_g^2} \partial_t^2 \right) \boldsymbol{\psi}_\epsilon - \tfrac{g(\boldsymbol{\psi})}{2} \left(1 + \tfrac{1}{\Omega_g^2} \partial_t^2 \right) \boldsymbol{\psi} \right\} \\ &\quad + \lim_{\epsilon \to 0} \tfrac{1}{\epsilon} \left\{ \left(-\tfrac{\beta}{2} \mathbf{J} \partial_t^2 + \gamma(\psi_{\epsilon,1}^2 + \psi_{\epsilon,2}^2)\mathbf{J} \right) \boldsymbol{\psi}_\epsilon - \left(-\tfrac{\beta}{2} \mathbf{J} \partial_t^2 + \gamma(\psi_1^2 + \psi_2^2)\mathbf{J} \right) \boldsymbol{\psi} \right\}. \end{aligned} \tag{S6}$$

To simplify the first term on right hand side of Eq. (S6), we observe that

$$g(\boldsymbol{\psi}_\epsilon) = g(\boldsymbol{\psi}) - \tfrac{2\epsilon g^2(\boldsymbol{\psi})}{g_0 E_{\text{sat}}} \int_{-\infty}^{\infty} \boldsymbol{\psi}^T(t) \boldsymbol{u}(t) dt. \tag{S7}$$

Therefore,

$$\begin{aligned} &\tfrac{g(\boldsymbol{\psi}_\epsilon)}{2} \left(1 + \tfrac{1}{\Omega_g^2} \partial_t^2 \right) \boldsymbol{\psi}_\epsilon - \tfrac{g(\boldsymbol{\psi})}{2} \left(1 + \tfrac{1}{\Omega_g^2} \partial_t^2 \right) \boldsymbol{\psi} \\ &= \tfrac{\epsilon g(\boldsymbol{\psi})}{2} \left(1 + \tfrac{1}{\Omega_g^2} \partial_t^2 \right) \boldsymbol{u} - \left(\tfrac{\epsilon g^2(\boldsymbol{\psi})}{g_0 E_{\text{sat}}} \int_{-\infty}^{\infty} \boldsymbol{\psi}^T \boldsymbol{u} dt \right) \left(1 + \tfrac{1}{\Omega_g^2} \partial_t^2 \right) \boldsymbol{\psi}. \end{aligned} \tag{S8}$$

Simplifying the second term on the right hand side of Eq. (S6), we obtain

$$\begin{aligned} &\left(-\tfrac{\beta}{2} \mathbf{J} \partial_t^2 + \gamma(\psi_{\epsilon,1}^2 + \psi_{\epsilon,2}^2)\mathbf{J} \right) \boldsymbol{\psi}_\epsilon - \left(-\tfrac{\beta}{2} \mathbf{J} \partial_t^2 + \gamma(\psi_1^2 + \psi_2^2) 2\mathbf{J} \right) \boldsymbol{\psi} \\ &= -\tfrac{\epsilon\beta}{2} \mathbf{J} \partial_t^2 \boldsymbol{u} + \epsilon\gamma(\psi_1^2 + \psi_2^2)\mathbf{J}\boldsymbol{u} + 2\epsilon\gamma \mathbf{J} \boldsymbol{\psi} \boldsymbol{\psi}^T \boldsymbol{u}. \end{aligned} \tag{S9}$$

Substituting Eq. (S8) and Eq. (S9) in Eq. (S6), we find that the linearized transfer function, $\mathcal{U}^{\text{FA}}$, is given by

$$\mathbf{u}_{\text{out}} = \mathcal{U}^{\text{FA}} \mathbf{u}_{\text{in}}, \tag{S10}$$

where $\mathbf{u}_{\text{out}} = \mathbf{u}(\text{L}_{\text{FA}}, t)$ is obtained by solving the linearized initial value problem

$$\begin{aligned} &\partial_z \boldsymbol{u} = \left(g(\boldsymbol{\psi})\mathbf{K} + \mathbf{L} + \mathbf{M}_1(\boldsymbol{\psi}) + \mathbf{M}_2(\boldsymbol{\psi}) \right) \boldsymbol{u} + \mathbf{P}(\boldsymbol{\psi})(\boldsymbol{u}), \\ &\mathbf{u}(0, t) = \mathbf{u}_{\text{in}}, \end{aligned} \tag{S11}$$

where

$$\begin{aligned} \mathbf{K} &= \tfrac{1}{2} \left(1 + \tfrac{1}{\Omega_g^2} \tfrac{\partial^2}{\partial t^2} \right), \\ \mathbf{L} &= -\tfrac{\beta}{2} \mathbf{J} \partial_t^2, \\ \mathbf{M}_1(\boldsymbol{\psi}) &= \gamma(\psi_1^2 + \psi_2^2)\text{J}, \\ \mathbf{M}_2(\boldsymbol{\psi}) &= 2\gamma \text{J} \boldsymbol{\psi} \boldsymbol{\psi}^T, \end{aligned} \tag{S12}$$

and

$$\mathbf{P}(\boldsymbol{\psi})(\boldsymbol{u}) = -\tfrac{g^2(\boldsymbol{\psi})}{g_0 E_{\text{sat}}} \left(\left(1 + \tfrac{1}{\Omega_g^2} \tfrac{\partial^2}{\partial t^2} \right) \boldsymbol{\psi} \right) \int_{-\infty}^{\infty} \boldsymbol{\psi}^T(t) \boldsymbol{u}(t) dt \tag{S13}$$

is a nonlocal operator. When we discretize the time window, $[-T/2, T/2]$, the vector-valued functions, $\boldsymbol{\psi}$ and $\boldsymbol{u}$, are replaced by column vectors in the $2N$-dimensional Euclidean space, $\mathbb{R}^{2N}$, which we also denote by $\boldsymbol{\psi}$ and $\boldsymbol{u}$. Then, the discretization of the nonlocal operator $\mathbf{P}(\boldsymbol{\psi})$ is given by the matrix-vector multiplication

$$\mathbf{P}(\boldsymbol{\psi})\boldsymbol{u} = -\tfrac{g^2(\boldsymbol{\psi})\Delta t}{g_0 E_{\text{sat}}} \left(\left(1 + \tfrac{1}{\Omega_g^2} \tfrac{\partial^2}{\partial t^2} \right) \boldsymbol{\psi} \right) \boldsymbol{\psi}^T \boldsymbol{u}. \tag{S14}$$

The linearized transfer function of a single mode fiber segment can be obtained by setting $g_0 = 0$ in the derivation above.

We now derive the linearized transfer function for the saturable absorber, $\mathcal{U}^{\mathrm{SA}}$. The transfer function, $\mathcal{P}^{\mathrm{SA}}$, of the saturable absorber is given by

$$\boldsymbol{\psi}_{\mathrm{out}} = \mathcal{P}^{\mathrm{SA}}(\boldsymbol{\psi}_{\mathrm{in}}) = (1 - \ell(\boldsymbol{\psi}_{\mathrm{in}}))\, \boldsymbol{\psi}_{\mathrm{in}}, \tag{S15}$$

where

$$\ell(\boldsymbol{\psi}_{\mathrm{in}}) = \frac{\ell_0}{1 + (\psi_{\mathrm{in},1}^2 + \psi_{\mathrm{in},2}^2)/P_{\mathrm{sat}}}. \tag{S16}$$

We use the perturbation $\boldsymbol{\psi}_{\mathrm{in},\epsilon} = \boldsymbol{\psi}_{\mathrm{in}} + \epsilon \mathbf{u}_{\mathrm{in}}$ to linearize $\mathcal{P}^{\mathrm{SA}}$ about $\boldsymbol{\psi}_{\mathrm{in}}$. Here, $\boldsymbol{\psi}_{\mathrm{in},\epsilon}$ and $\boldsymbol{\psi}_{\mathrm{in}}$ satisfy Eq. (S15). Therefore, we obtain

$$\begin{aligned}
\mathbf{u}_{\mathrm{out}} &= \lim_{\epsilon \to 0} \frac{\boldsymbol{\psi}_{\mathrm{in},\epsilon} - \boldsymbol{\psi}_{\mathrm{in}}}{\epsilon} \\
&= \lim_{\epsilon \to 0} \frac{1}{\epsilon} \left\{ \left(1 - \ell(\boldsymbol{\psi}_{\mathrm{in},\epsilon})\right) \boldsymbol{\psi}_{\mathrm{in},\epsilon} - (1 - \ell(\boldsymbol{\psi}_{\mathrm{in}}))\, \boldsymbol{\psi}_{\mathrm{in}} \right\} \\
&= \lim_{\epsilon \to 0} \left\{ \mathbf{u}_{\mathrm{in}} - \ell(\boldsymbol{\psi}_{\mathrm{in},\epsilon}) \mathbf{u}_{\mathrm{in}} - \frac{\ell(\boldsymbol{\psi}_{\mathrm{in},\epsilon}) - \ell(\boldsymbol{\psi}_{\mathrm{in}})}{\epsilon} \boldsymbol{\psi}_{\mathrm{in}} \right\}.
\end{aligned} \tag{S17}$$

Next, we use Eq. (S16) to obtain

$$\ell(\boldsymbol{\psi}_{\mathrm{in},\epsilon}) = \ell(\boldsymbol{\psi}_{\mathrm{in}}) - \frac{2\epsilon \ell^2(\boldsymbol{\psi}_{\mathrm{in}})}{\ell_0 P_{\mathrm{sat}}} \boldsymbol{\psi}_{\mathrm{in}}^T \mathbf{u}_{\mathrm{in}}. \tag{S18}$$

Using Eq. (S18) in Eq. (S17), we finally obtain the linearized transfer function, $\mathcal{U}^{\mathrm{SA}}$, given by

$$\mathbf{u}_{\mathrm{out}} = \mathcal{U}^{\mathrm{SA}}(\boldsymbol{\psi}_{\mathrm{in}})(\mathbf{u}_{\mathrm{in}}) = \left(1 - \ell(\boldsymbol{\psi}_{\mathrm{in}}) - \frac{2\ell^2(\boldsymbol{\psi}_{\mathrm{in}})}{\ell_0 P_{\mathrm{sat}}} \boldsymbol{\psi}_{\mathrm{in}} \boldsymbol{\psi}_{\mathrm{in}}^T \right) \mathbf{u}_{\mathrm{in}}. \tag{S19}$$

The remaining components, i.e. dispersion compensation fiber and output coupler, already have linear transfer functions.

3. ADDITIONAL NUMERICAL RESULTS

In the paper, we showed numerical results for two parameter sets, the first with a weaker saturable absorber ($\ell_0 = 0.1$, $P_{\mathrm{sat}} = 2000$ W) and the second with a stronger saturable absorber ($\ell_0 = 0.2$, $P_{\mathrm{sat}} = 50$ W). We chose these two parameter sets because with the first set the pulse is unstable and with the second set it is stable, and in both cases the stability of the pulse is determined by the essential spectrum rather than by the discrete eigenvalues. This is because for both parameter sets the largest magnitude of the points in the continuous spectrum always exceeds the magnitudes of the discrete eigenvalues. In this section, we present additional numerical results showing bifurcations from an unstable to a stable pulse by varying ℓ_0 and P_{sat} one at a time. First, we fix $\ell_0 = 0.05$ and decrease the value of P_{sat} from 1000 W to 200 W. Then, we fix $P_{\mathrm{sat}} = 500$ W and increase ℓ_0 from 0.02 to 0.14. The other components of the laser have the same parameter values as given in Sec. 2 of the paper. From Eq. (6), we observe that as P_{sat} decreases, the loss near the center of the pulse increases, since the saturation absorption effect is stronger. Similarly, as ℓ_0 increases, the loss near the center of the pulse increases. For these parameter variations, as we vary P_{sat} or ℓ_0, the stability of the pulse is determined by the continuous spectrum, since the largest magnitude of the points in the continuous spectrum always exceeds the magnitudes of the discrete eigenvalues.

In Fig. S2, we show results for $P_{\mathrm{sat}} = 1000$ W (top row), $P_{\mathrm{sat}} = 300$ W (middle row) and $P_{\mathrm{sat}} = 200$ W (bottom row). In all three cases, we chose $\ell_0 = 0.05$. In the top left panel, we show the amplitude of the pulse at the output coupler as computed using the evolutionary method after 100 round trips (solid blue) and using the optimization method (dashed red). The small wings on the sides of the pulse computed using the evolutionary method suggest that this pulse is unstable. In the middle panel of the first row, we show the set of all eigenvalues of the discretized monodromy matrix, $\mathbf{M}$, (blue circles) and the continuous spectrum, $\sigma_{\mathrm{cont}}(\mathcal{M})$, obtained using the formula given in the paper (solid red), both computed for the optimized pulse with $P_{\mathrm{sat}} = 1000$ W. In the right panel, we show excellent agreement between the two spectra in a small neighbourhood of $\lambda = 1$. The largest eigenvalue on the real axis is $\lambda = 1.0146$ as obtained using the formula for the continuous spectrum and $\lambda = 1.0145$ as obtained using the numerical method. Therefore, the spectral method shows that the pulse is indeed unstable. To further verify this result, we propagated the perturbed pulse, $\boldsymbol{\psi}_\epsilon = \boldsymbol{\psi} + \epsilon \boldsymbol{u}$, through the system, where $\epsilon = 10^{-5}$ and $\boldsymbol{u}$ is the normalized eigenvector corresponding to the eigenvalue with largest magnitude. In the top row of Fig. S3, we show the pulse, $\boldsymbol{\psi}_\epsilon$, after 4000 round trips, on a linear scale (left) and logarithmic scale (right) , together with the optimized pulse. The relative L^2 error between these two pulses is 0.9837.

In the center rows of Fig. S2 and Fig. S3, we show the corresponding results for $P_{\mathrm{sat}} = 300$ W. In this case, the wings on the sides of the pulse obtained with the evolutionary method (solid blue) are not as pronounced. The spectral method shows that the pulse is unstable since the largest eigenvalue on the real axis is $\lambda = 1.0013$ as obtained both using the

formula and with the numerical method. The relative L^2 error of between the evolved perturbed pulse, ψ_ϵ, and the optimized pulse is 0.7494. In the left panel of Fig. S4, we plot the largest eigenvalue as a function of P_{sat}. We observe that this eigenvalue remains outside the unit circle as P_{sat} decreases from 1000 W and 300 W. Therefore, the pulse is unstable over this range of values of P_{sat}.

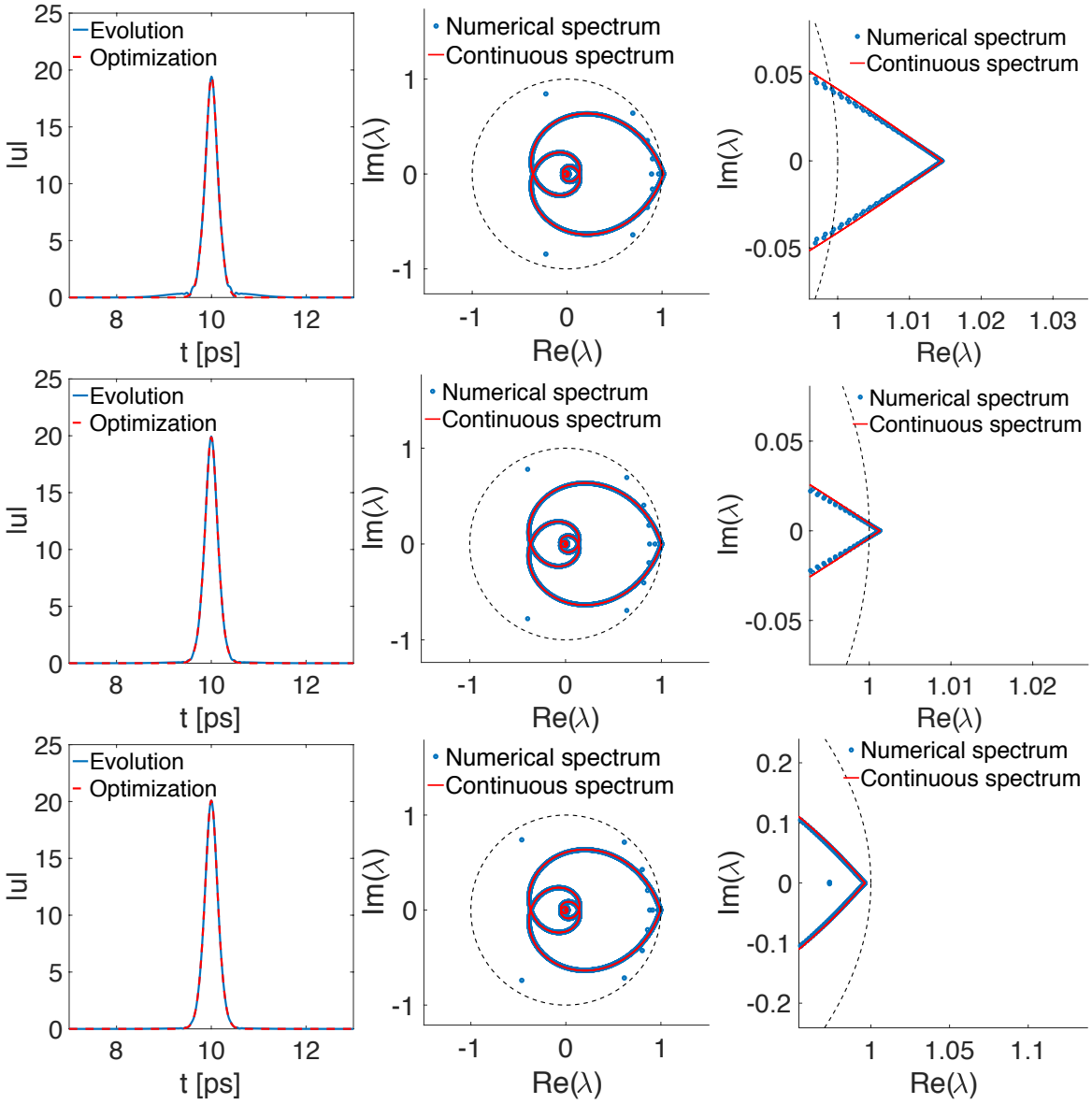

Fig. S2. Top row: Left: Periodically stationary pulses obtained using the evolutionary approach (solid blue) and optimization (dashed red) for $P_{\text{sat}} = 1000$ W. **Center and right:** Eigenvalues of the discretized monodromy matrix, $\mathbf{M}$, (blue circles) and the continuous spectrum, $\sigma_{\text{cont}}(\mathcal{M})$, computed using the formula given in paper (solid red) for optimized pulse. **Center and bottom rows:** Corresponding results for $P_{\text{sat}} = 300$ W and $P_{\text{sat}} = 200$ W, respectively. In all three cases, $\ell_0 = 0.05$.

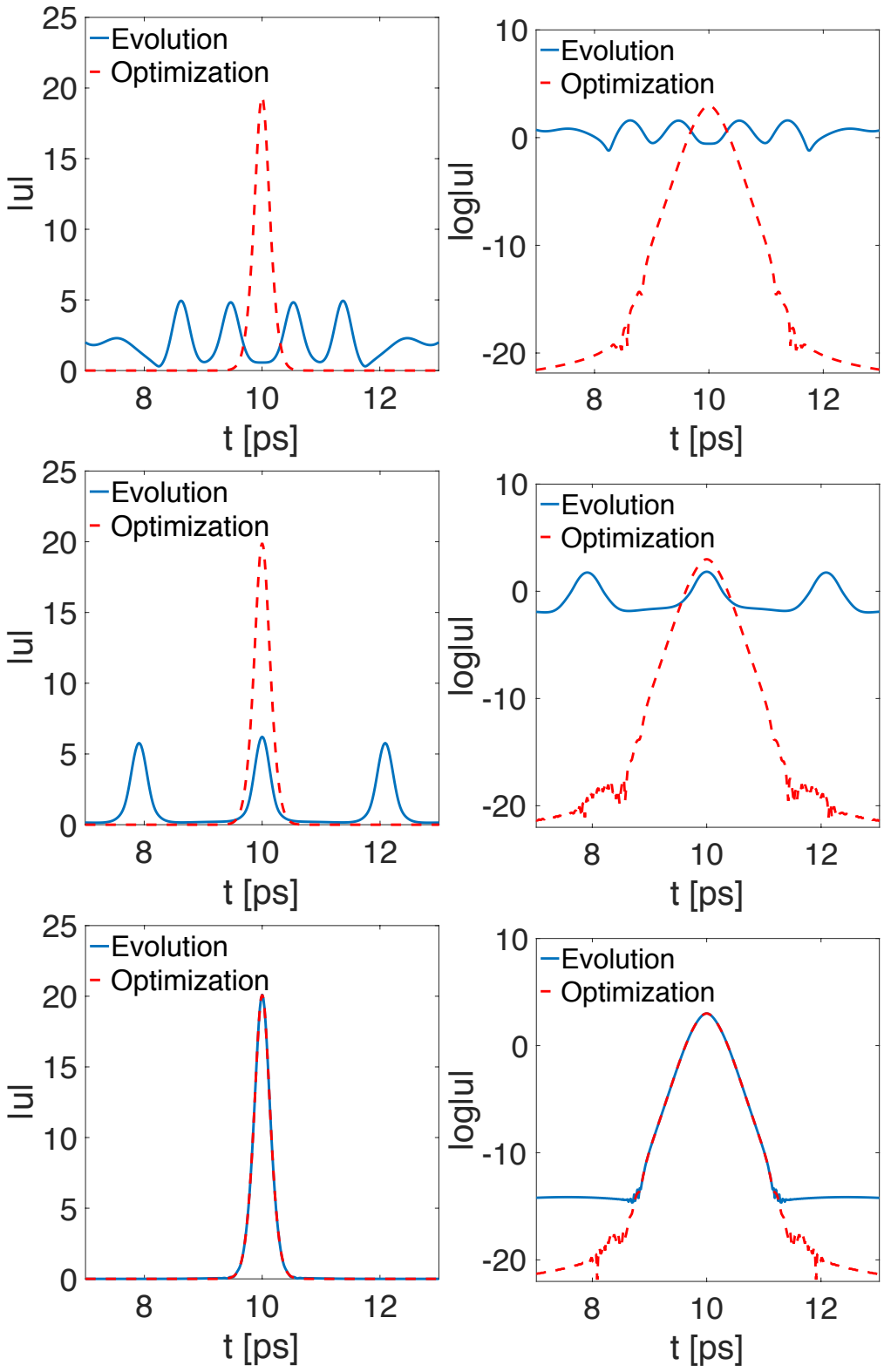

Fig. S3. Top row: Left: Perturbed optimized pulse, ψ_ϵ, at the output coupler after evolution over 4000 round trips (solid blue) and the optimized pulse (dashed red) for $P_{\text{sat}} = 1000$ W. **Right:** Corresponding results on a log scale. **Center and bottom rows:** Corresponding results for $P_{\text{sat}} = 300$ W and $P_{\text{sat}} = 200$ W, respectively. In all three cases, $\ell_0 = 0.05$.

In the bottom rows of Fig. S2 and Fig. S3, we show the corresponding results for $P_{\text{sat}} = 200$ W. In this case, the periodically stationary pulse obtained using the evolutionary method agrees very well with the one obtained using the optimization method. Further, the spectrum of the optimized pulse lies inside the unit circle with the largest eigenvalue on the real axis $\lambda = 0.99618$ as obtained using the formula and $\lambda = 0.99616$ as obtained using the numerical method. Finally, the evolved perturbed pulse, $\boldsymbol{\psi}_\epsilon$, also agrees very well with the optimized pulse with the relative L^2 error 3.9005×10^{-4}. Therefore, using these observations we conclude that when $P_{\text{sat}} = 200$ the periodically stationary pulse is stable. In conclusion, these results show that as the saturation absorption effect becomes stronger, the pulse transitions from being unstable to being stable.

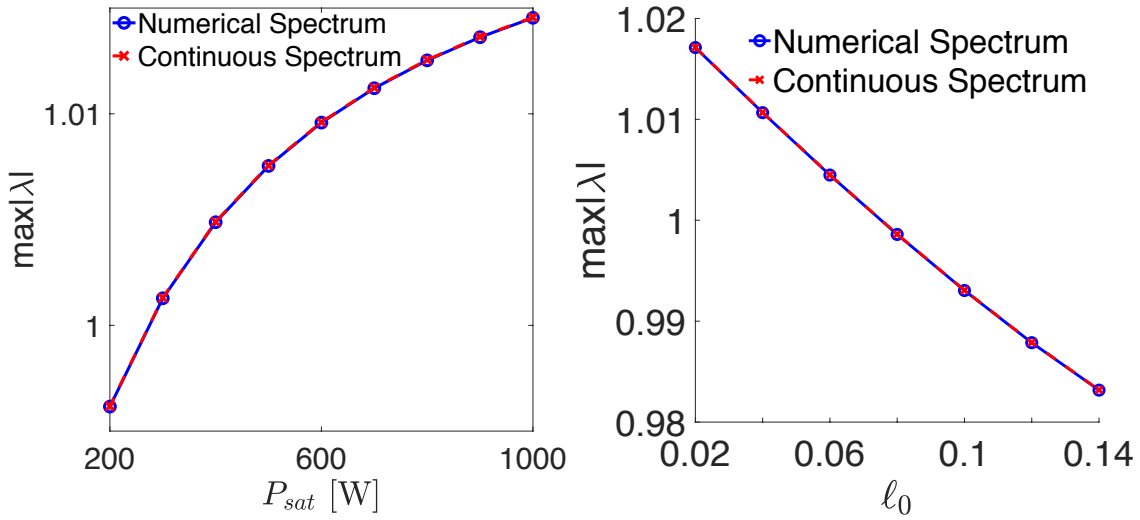

Fig. S4. Left: A plot of the maximum real eigenvalue, $\max|\lambda|$, vs. P_{sat} showing a bifurcation from a stable to an unstable pulse. Here, $\ell_0 = 0.05$. Right: Corresponding plot in which ℓ_0 is varied and $P_{\text{sat}} = 500$ W.

In Fig. S5, we present results similar to Fig. S2 for $\ell_0 = 0.02$ (top row), $\ell_0 = 0.06$ (middle row) and $\ell_0 = 0.08$ (bottom row). In all three cases, $P_{\text{sat}} = 500$ W. In the top left panel, the small wings on the sides of the pulse computed using the evolutionary method suggest that this pulse is unstable. The largest eigenvalue on the real axis is $\lambda = 1.0171$ as obtained using the formula for the continuous spectrum as well as using the numerical method. Therefore, the spectral method shows that the pulse is indeed unstable.

In the center rows of Fig. S5, we show the corresponding results for $\ell_0 = 0.06$. In this case, the wings on the sides of the pulse obtained with the evolutionary method (solid blue) are not as pronounced. The spectral method shows that the pulse is unstable since the largest eigenvalue on the real axis is $\lambda = 1.0045$ as obtained using both the methods. Since the maximum eigenvalue remains outside the unit circle as ℓ_0 increases from 0.02 to 0.06, the pulse is unstable over this range of values of ℓ_0. This behavior is also shown in the right panel of Fig. S4, where we plot the largest eigenvalue as a function of ℓ_0.

In the bottom rows of Fig. S5, we show the corresponding results for $\ell_0 = 0.08$. In this case, the periodically stationary pulse obtained using the evolutionary method agrees very well with the one obtained using the optimization method. Further, the spectrum of the optimized pulse lies inside the unit circle with the largest eigenvalue on the real axis $\lambda = 0.99862$ as obtained using the formula and $\lambda = 0.99859$ as obtained using the numerical method. Therefore, we conclude that the periodically stationary pulse associated with $\ell_0 = 0.08$ is stable. From the plot in the right panel of Fig. S4, we observe that the periodically stationary pulses remain stable as ℓ_0 increases from 0.08 to 0.14. In conclusion, these results show that as the saturation absorption effect becomes stronger, the pulse transitions from being unstable to being stable.

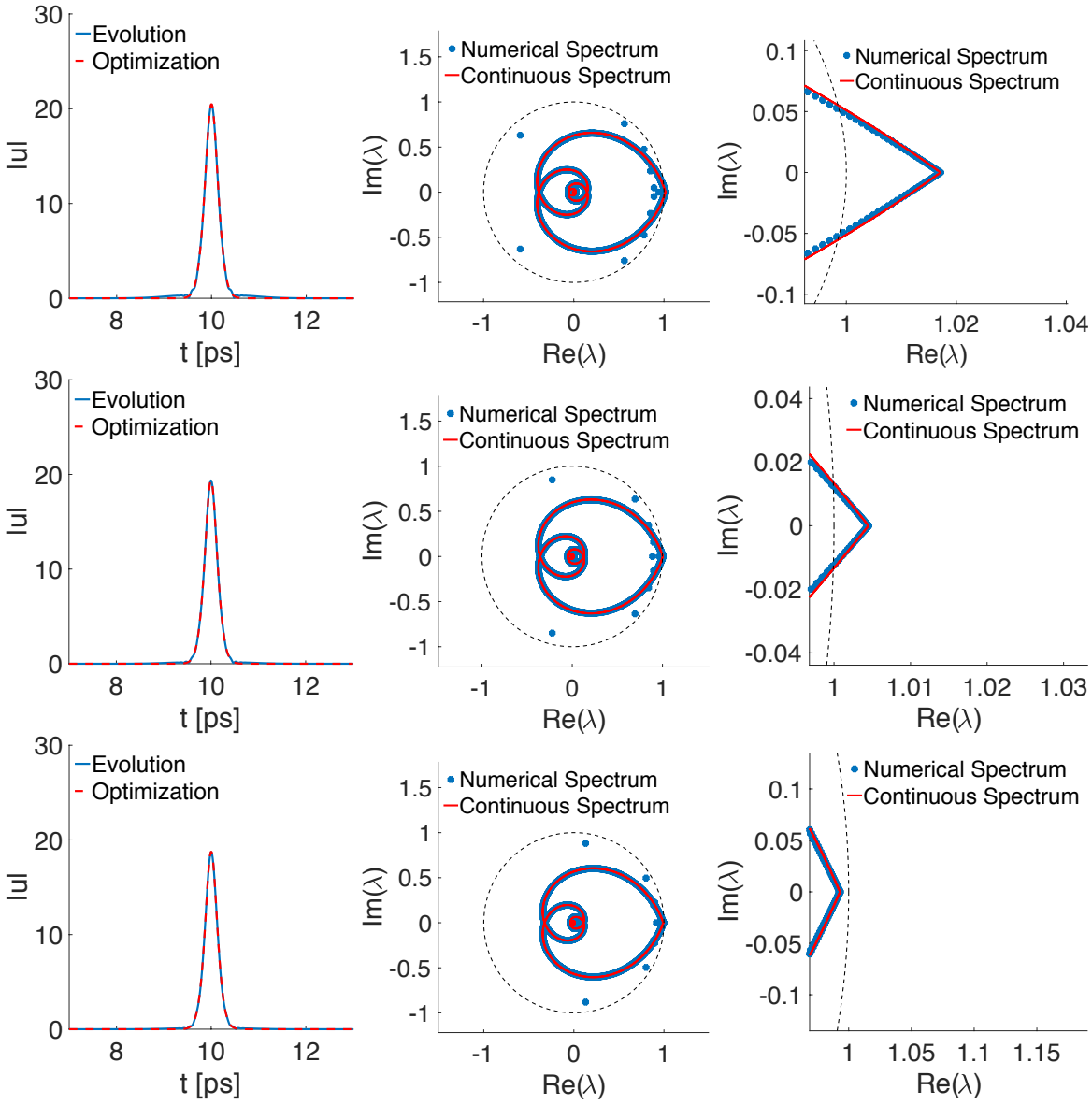

Fig. S5. Top row: Left: Periodically stationary pulses obtained using the evolutionary approach (solid blue) and optimization (dashed red) for $\ell_0 = 0.02$. **Center and right:** Eigenvalues of the discretized monodromy matrix, $\mathbf{M}$, (blue circles) and the continuous spectrum, $\sigma_{\text{cont}}(\mathcal{M})$, computed using the formula given in paper (solid red) for optimized pulse. **Center and bottom rows:** Corresponding results for $\ell_0 = 0.06$ and $\ell_0 = 0.08$, respectively. In all three cases, $P_{\text{sat}} = 500$ W.